CHALMERS

Design and Performance of Carrier-Based Direct-Sequence Ultra-Wideband Systems

MATTS-OLA WESSMAN, ARNE SVENSSON, AND ERIK AGRELL

Communication Systems Group
Department of Signals and Systems
Chalmers University of Technology
Göteborg, Sweden, 2005

R013/2005
ISSN 1403-266X

Design and Performance of Carrier-Based Direct-Sequence Ultra-Wideband Systems

Matts-Ola Wessman, Arne Svensson,
and Erik Agrell

CHALMERS

Communication Systems Group
Department of Signals and Systems
Chalmers University of Technology
Göteborg 2005

Published in April 2005 as
Design and Performance of Carrier-Based Direct-Sequence
Ultra-Wideband Systems
Technical Report No. R013/2005
Communication System Group
Department of Signals and Systems
Chalmers University of Technology
SE-412 96 Gothenburg, Sweden
Telephone: +46 (0)31-772 1000

Printed by Department of Signals and Systems,
Chalmers University of Technology
SE-412 96 Gothenburg, Sweden in April 2005

Abstract

A set of physical layer specifications is provided for a single-band and a dual-band system. Both systems fulfill the FCC regulations on UWB devices. The single-band system gives reliable communication, i.e., a 90th-percentile PER less than 8% for 1024 payload bytes, at 110 Mbps with a transmitter–receiver separation of up to 10 meters on the IEEE 802.15.3a channel model CM4. 205 Mbps at 6.7 meters on CM4 and 513 Mbps at 3.8 meters on CM2 were also obtained, and thus the requirements from IEEE 802.15.3a are fulfilled. The single-band system uses the spectrum 3.1–4.9 GHz, a chip-spaced rake combiner with 60 fingers, and a sliding window (SW) channel estimator. The sampling rate is 1540 Msamples/s.

The dual-band system uses two bands, 3.1–4.0 GHz and 4.0–4.9 GHz. The system has the same sampling rate of 1540 Msamples/s and uses a fractionally spaced rake combiner. The system offers 10.2 meters on CM3 in the lower 3.1–4.0 GHz band when combining all available multipath components that have been perfectly estimated. When using 16 rake fingers and the SW algorithm, 7.7 meters is obtained in the lower band on CM3. For CM4 and the upper bands, the obtained distances are less than 8.5 meters, even with perfect channel estimation.

A channel impulse response gain is defined as a function of the Fourier transform of the channel impulse response. It is shown that this gain, which is a random variable, can be approximated by the multiplication of two other random variables that have a log-normal and a gamma distribution, respectively.

Contents

1 Introduction

In the near future, there will appear a demand for low cost, high-speed, wireless links for short range (< 10 m) communication. Ultra-wideband (UWB) systems could provide those features. UWB systems can be classified to be either single band or multiband and to use either carrier based radio or impulse radio. FCC restricted that UWB devices have to use at least 500 MHz instantaneous bandwidth in the 3.1–10.6 GHz band with a power spectral density of at most –41.25 dBm/MHz [1]. This leads to very low transmit power.

Within the IEEE 802.15 working group for wireless personal area network (WPAN), the standardization of an alternative, high rate, physical layer, denoted 802.15.3a, is ongoing. The result after the down selection of several proposals are two merged proposals. The first is denoted multiband-OFDM (MB-OFDM) and the second is denoted DS-UWB [2–5]. The DS-UWB system uses two bands with BPSK or quaternary bi-orthogonal keying (4BOK). A new UWB channel model based on the Saleh–Valenzuela model was adopted and used in the evaluation of the several physical layer proposals [6, 7].

In parallel to the 802.15.3a standardization, the EU research project, Ultrawaves, investigated UWB from, e.g, physical layer, MAC layer, antennas, and channel modeling points of view. Coherent and noncoherent impulse radio systems with 100 Mbps and repetition codes were compared on the IEEE 802.15.3a channel model. Both systems used higher-order derivatives of the Gaussian pulse in order to comply with the FCC regulations. The physical layer was decided to be a coherent, single-band system using up- and down-converters. See [8–11] for details.

The first objective of this paper is to find the system specification for a single-band, coherent, carrier-based direct-sequence spread-spectrum (DS-SS) system that fulfills the physical layer requirements from IEEE 802.15.3a. Based on [6, 12, 13], the investigated system should provide at least a payload bit rate of 110 Mbps at 10 meters and at least 200 Mbps at 4 meters. An optional requirement is at least 480 Mbps at 2 meters. The packet error rate (PER) should be less than or equal to 8% for a payload of 1024 information bytes per packet. The system should also fulfill the FCC regulations on UWB devices. The second objective is to investigate a dual-band system that uses the same spectrum and sampling rate as the single-band system.

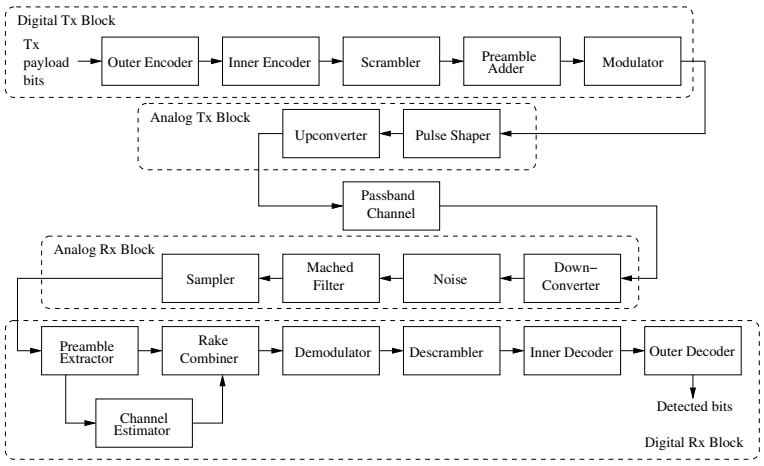

Figure 1: The system model of the investigated system.

2 System Model

Fig. 1 depicts the system model that consists of a digital transmitter block, an analog transmitter block, a channel, an analog receiver block, and a digital receiver block.

2.1 Transmitter–Receiver Algorithms

2.1.1 Digital Transmitter Block

The digital transmitter encodes first N_i information bits per packet using an outer convolutional code with rate $k_{\mathrm{CC}}/n_{\mathrm{CC}}$ and an inner repetition code with rate $1/n_{\mathrm{rep}}$. Then the encoded bits are scrambled. The payload of a packet is defined here to be the scrambled encoded bits. Then N_p known pseudo-white pilots are added as a preamble before the payload. Finally, the signal is quadrature modulated with $\log_2 M$ bits per chip, where M is the constellation size.

The concatenated code has code rate k/n where $k = k_{\mathrm{CC}}$ and $n = n_{\mathrm{CC}} n_{\mathrm{rep}}$. The number of payload chips and pilot chips per packet are $N_i n/(k \log_2 M)$ and $N_p/\log_2 M$, respectively. If R_c is the chip rate, then the payload bit rate is given by $R_b = kR_c \log_2 M/n$. The duration of one chip is $T_c = 1/R_c$.

2.1.2 Analog Transmitter and Receiver Blocks

In the analog transmitter block, the complex modulated chips from the digital transmitter block are pulse shaped and upconverted to carrier frequency f_c. In the analog receiver block, the passband signal from the channel is downconverted to baseband. Complex

front end receiver noise is added, before the signal is pulse-matched filtered. Finally, the signal is sampled with a sampling time T_{samp}.

2.1.3 Digital Receiver Block

The digital receiver has a preamble extractor, a channel estimator, a rake combiner, a demodulator, a descrambler, an inner decoder, and an outer decoder. After finding the preamble, the channel estimator estimates the complex baseband representation of the impulse response of the passband channel with a sliding window (SW) algorithm. The estimator cross-correlates the received pilot sequence and the transmitted pilot sequence. Then it finds the N_R complex-valued gains $\{\hat{a}_l\}$ and delays $\{\hat{\tau}_l\}$ that correspond to the N_R largest amplitudes of the cross-correlated sequence. Each delay $\hat{\tau}_l$ is an integer times the sampling time T_{samp}.

A selective rake combiner is used to equalize the received payload. The signals in the N_R strongest rake fingers are combined in a maximum ratio fashion (MRC). The equalized signal is then demodulated into a real-valued stream and descrambled. The inner repetition decoder is a soft-input soft-output decoder, which adds up the received amplitudes corresponding to n_{rep} coded bits. The outer Viterbi decoder uses soft-decision decoding.

A chip-spaced (CS) receiver samples the signal in the analog receiver block with a rate equal to the chip rate, i.e, $T_{\text{samp}} = 1/R_c$, which normally introduces aliasing. A fractionally spaced (FS) receiver avoids the aliasing by sampling at least as fast as the Nyquist rate [14]. In a fractionally spaced digital-receiver block, the channel estimator and the rake combiner work at the higher rate. The last step in the rake combiner is to downsample the equalized signal to chip rate.

2.2 Channel Models

2.2.1 Free Space Channel or the AWGN Channel

A flat, time-static channel with free space propagation loss and only additive white gaussian noise (AWGN) is here referred to as the AWGN channel or the free space channel. The impulse response $h(t) = \delta(t)$. A channel impulse response (CIR) gain G_{CIR} is defined to be given by

$$G_{\text{CIR}} = \int_0^\infty |V(f - f_c)H(f)|^2 \, df, \tag{1}$$

where $V(f)$ is the continuous-time Fourier transform (CTFT) of the transmitted waveform that is normalized so that $\int_{-\infty}^{\infty} |V(f)|^2 \, df = 1$.

Further, f_c is the carrier frequency and $H(f)$ is the CTFT of $h(t)$. This definition does not consider the free space path loss. For the AWGN channel, G_{CIR} is always one. Assume that the waveform can be approximated with a brick-wall filter with bandwidth B, then the gain can be approximated with

$$G_{\mathrm{CIR}} \approx \frac{1}{B} \int_{f_c-B/2}^{f_c+B/2} |H(f)|^2 \, df. \tag{2}$$

2.2.2 IEEE 802.15.3a Channel Model

The IEEE 802.15.3a channel model is a stochastic channel model, where a new channel impulse response $h(t)$ is drawn for every connection. Each CIR, i.e, each realization of the channel model, is generated independently from previously generated CIRs.

The model is assumed to be time-invariant during a connection. The CIR is identical even for a packet that has been retransmitted by the automatic repeat request (ARQ) scheme due to a packet error. The channel is block-fading, where the time duration of a block is the same as the duration of a connection.

Clearly, for a certain transceiver algorithm setup and signal-to-noise ratio (SNR), the PER is a function of the CIR. A receiver suffers from different PERs during different connections. Due to the block fading property, this motivates the use of PER measures based on the probability of having a connection. Two PER measures can be defined by discarding the 10% worst channels, the 90th-percentile PER and the mean PER of the 90% best channels, which are denoted by PER_{90} and $\overline{\mathrm{PER}}_{90}$, respectively. With a 90% probability, the obtained PER on a connection is lower than or equal to the 90th-percentile PER and is defined with

$$\mathbb{P}\left(\mathrm{PER} < \mathrm{PER}_{90}\right) = 0.9. \tag{3}$$

The mean PER of the 90% best channels is given by

$$\overline{\mathrm{PER}}_{90} = \int_{0}^{\mathrm{PER}_{90}} p \, \frac{f_{\mathrm{PER}}(p)}{0.9} \, dp, \tag{4}$$

where $f_{\mathrm{PER}}(p)$ is the pdf of the PER.

The block-fading property discourages the use of a mean PER measure. A receiver will suffer from the mean PER if packets are transmitted and retransmitted over independently generated CIRs. The mean PER is given by

$$\overline{\mathrm{PER}} = \mathbb{E}\left(\mathrm{PER}\right) = \int_{0}^{\infty} p \, f_{\mathrm{PER}}(p) \, dp. \tag{5}$$

Also, since there is no randomness in the CIR of the AWGN channel, there is only one PER. Thus, it is meaningless to define or discuss mean PER or PER_{90} on the AWGN channel.

The IEEE 802.15.3a channel model is based on the Saleh–Valenzuela model where multipath components arrive in clusters [6, 7]. This multipath channel can be expressed as

$$h(t) = Xc(t) = \frac{X}{\sqrt{G_\alpha}} \sum_{l=0}^{\infty} \sum_{k=0}^{\infty} \alpha_{k,l} \delta(t - T_l - \tau_{k,l}), \tag{6}$$

where the real-valued multipath gain is defined by $\alpha_{k,l}$ for cluster l and ray k. The lth cluster arrives at T_l and its kth ray arrives at $\tau_{k,l}$, which is relative to the first path in cluster l, i.e., $\tau_{0,l} = 0$. X denotes log-normal shadowing. Further,

$$G_\alpha = \sum_{k,l} |\alpha_{k,l}|^2. \tag{7}$$

The random variables $\{\alpha_{k,l}\}$ are generated independently but are not identically distributed. The expected value $\mathbb{E}\left(|\alpha_{k,l}|^2\right)$ is proportional to $\exp\left(-T_l/\Gamma - \tau_{k,l}/\gamma\right)$, where Γ and γ denote a cluster- and a ray-decay factor, respectively. The amplitude $|\alpha_{k,l}|$ has a log-normal distribution since the clusters and the rays fade with two independent log-normally distributed random variables. The standard deviations of the two corresponding normally distributed random variables are σ_1 and σ_2, respectively. Further, the phase $\angle\alpha_{k,l}$ is chosen from $\{0, \pi\}$ with equal probability. The log-normal shadowing is modeled with $X = 10^{n/20}$, where n has a normal distribution with mean $\mu_n = 0$ and standard deviation $\sigma_n = 3$. This is denoted by $n \sim N(\mu_n, \sigma_n^2)$.

The arrival times of the clusters and the rays within one cluster are given by two independent Poisson processes with intensities Λ and λ, respectively. In other words, the interarrival times between two clusters $T_{l+1} - T_l$ and two rays within one cluster $\tau_{k+1,l} - \tau_{k,l}$ are exponentially distributed with

$$p(T_{l+1}|T_l) = \Lambda \exp\left(-\Lambda(T_{l+1} - T_l)\right) \tag{8}$$

and

$$p(\tau_{k+1,l}|\tau_{k,l}) = \lambda \exp\left(-\lambda(\tau_{k+1,l} - \tau_{k,l})\right), \tag{9}$$

respectively. The arrival time of the first cluster T_0 is zero for line-of-sight (LOS) models and exponentially distributed with intensity Λ for nonline-of-sight (NLOS) models.

Since $h(t)$ is a random variable, then $H(f)$ is a random variable, and the channel impulse response gain G_{CIR} in (1) is also a random

variable for the IEEE 802.15.3a channel model. The distribution of G_{CIR} will be further discussed in Sec. 3. The continuous-time CIR in (6) is converted to a discrete-time CIR for a given target sampling frequency as described now. First the arrival times are quantized into bins with a time resolution less than 0.01 μs. This discrete-time CIR is then digitally antialias filtered and finally downsampled to the target sampling frequency. Tab. 1 gives the model parameters for the four models CM1, CM2, CM3, and CM4. See [6] for a more detailed explanation of the model.

Table 1: Parameters for the 802.15.3a channel model

	CM1	CM2	CM3	CM4	unit
Tx–Rx separation	0-4	0-4	4-10		m
(Non-)line of sight	LOS	NLOS	NLOS	NLOS	
Model Parameters					
Cluster arrival rate (Λ)	0.0233	0.4	0.0667	0.0667	1/ns
Ray arrival rate (λ)	2.5	0.5	2.1	2.1	1/ns
Cluster-decay factor (Γ)	7.1	5.5	14.00	24	
Ray-decay factor (γ)	4.3	6.7	7.9	12	
Cluster fading (σ_1)	3.3941	3.3941	3.3941	3.3941	dB
Ray fading (σ_2)	3.3941	3.3941	3.3941	3.3941	dB
Shadowing (σ_n)	3	3	3	3	dB
Model Characteristics					
Mean excess delay	5.0	9.9	15.9	30.1	ns
RMS delay spread	5	8	15	25	ns

2.3 Link Budget and Energy per Bit

There are two important outputs from a link budget, an Rx sensitivity Ψ and a link margin M_L. Also, the budget connects an energy per bit to a distance. The link budget here is adapted from [6] but, e.g, the G_{CIR}, a processing gain PG, and a overhead loss L_{OH} have been added. Let d be the transmitter–receiver (T–R) separation in meters. Then the received power is

$$P_r = P_{r,\mathrm{fs}} G_{\mathrm{CIR}} = \frac{P_t G_t G_r}{L_p(d)} G_{\mathrm{CIR}}, \tag{10}$$

where $P_{r,\text{fs}}$ is the received power and G_{CIR} is the channel impulse response gain in (1). Further, P_t is the average transmitted power, G_t is the transmitter antenna gain, and G_r is the receiver antenna gain. The power $P_{r,\text{fs}}$ is assumed to be given by the Friis free-space transmission equation with one modification. The path loss is given here by $L_p(d) = (4\pi d f_c'/c)^2$ where c is the speed of light and $f_c' = \sqrt{f_{\min} f_{\max}}$ where $f_{\min}$ and $f_{\max}$ are the -10 dB edges of the pulseform spectrum. The path loss coefficient n_{plc} is two.

The total noise power in the receiver is

$$P_N = N_{0,t} B_N N_F L_I, \tag{11}$$

where $N_{0,t} = -173.84$ dBm/Hz is the spectral density of the thermal noise, B_N is the noise bandwidth, N_F is the receiver noise figure, and L_I is the implementation loss. Further, the thermal noise power is $N_t = N_{0,t} B_N$ and the spectral density of the noise after despreading is $N_0 = N_{0,t} N_F L_I$. The implementation loss is the loss due to hardware impairments such as filter distortion, phase noise, quantization noise, and frequency errors that occur on the AWGN channel.

The received signal-to-noise ratio per payload bit, ε_{pb}/N_0, is defined to consider only the effects of coding and modulation, and to ignore the energy loss due to any preamble. Let $P_r = \varepsilon_{pb} R_b$ and the processing gain $\text{PG} = B_N/R_b$. Then

$$\frac{\varepsilon_{pb}}{N_0} = \frac{P_r}{P_N}\text{PG} = \frac{P_{r,\text{fs}}}{P_N} G_{\text{CIR}} \text{PG}. \tag{12}$$

Assuming that the noise bandwidth is equal to the chip rate, $B_N = R_c$, leads to $\text{PG} = n/(k \log_2 M)$. The minimum ε_{pb}/N_0 that a system requires to achieve a PER of 8 % on the AWGN channel is denoted Γ_{fs}. It is obtained with ideal hardware and synchronization since the hardware distortion is included in L_I.

The Rx sensitivity Ψ is the minimum mean received power that is required to give a PER of 8% on the AWGN channel at a certain distance d. The Rx sensitivity is given by

$$\Psi = \frac{\Gamma_{\text{fs}} P_N}{\text{PG}}. \tag{13}$$

The mean received power on the AWGN channel is $\bar{P}_{r,\text{AWGN}} = \mathbb{E}(P_r) = P_{r,\text{fs}}$ since $G_{\text{CIR}} = 1$. The link margin is given by $M_L = \bar{P}_{r,\text{AWGN}}/\Psi = P_{r,\text{fs}}/\Psi$. This link margin needs to be large enough so that the system also gives a 90th-percentile PER of 8% on the IEEE 802.15.3a channel models. It covers, e.g., additional implementation losses, imperfect channel estimation, imperfect multipath energy capture, and amplitude fading that occur on CM1–4, which was not considered in L_I.

The mean energy per information bit, E_b, is defined as the mean energy of one packet divided by the number of information bits per packet, N_i. This leads to

$$\frac{E_b}{N_0} = \mathbb{E}\left(\frac{\varepsilon_{pb}}{N_0} L_{\mathrm{OH}}\right) = \frac{P_{r,\mathrm{fs}}}{P_N} \mathbb{E}\left(G_{\mathrm{CIR}}\right) \mathrm{PG} L_{\mathrm{OH}}. \tag{14}$$

The overhead loss due to, e.g., pilots and any additional preamble, is given by $L_{\mathrm{OH}} = E_{\mathrm{Packet}}/E_{\mathrm{Payload}}$. Assuming that the preamble contains only N_p pilots and the same modulation is used for both the preamble and the payload, then $L_{\mathrm{OH}} = kN_p/(nN_i) + 1$. For an OFDM system, this overhead loss would also include the loss due to the cyclic prefix.

3 Distribution of the Gain of the CIR

The purpose of this section is to find the distribution of the channel impulse response gain G_{CIR} in (1) for the IEEE 802.15.3a channel model. The first step is to find the distribution of $|C(f)|^2$. The continuous-time Fourier transform of $h(t)$ in (6) is given by

$$H(f) = XC(f) = X \sum_{l=0}^{\infty} \sum_{k=0}^{\infty} \frac{\alpha_{k,l}}{\sqrt{G_\alpha}} \exp\left(-j2\pi f(T_l + \tau_{k,l})\right), \tag{15}$$

where the definition of $G_\alpha = \sum_{k,l} |\alpha_{k,l}|^2$ is repeated here for clarity. Let m be a bijective function with $m : \mathbb{N}_0^2 \mapsto \mathbb{N}_0$ and let $m = m(k,l)$. Then, $C(f)$ can be rewritten as

$$C(f) = \sum_{m=0}^{\infty} \beta_m \exp\left(-j2\pi f \tau_m\right), \tag{16}$$

where $\beta_m = \alpha_{k,l}/\sqrt{G_\alpha}$ and $\tau_m = T_l + \tau_{k,l}$. The random variables $\{\beta_m\}$ are dependent due to the division with $\sqrt{G_\alpha}$. Since T_l and $\tau_{k,l}$ are generated by independent Poisson processes, the random variables $\{\tau_m\}$ are independent. Also, $\{\tau_m\}$ and $\{\beta_m\}$ are independent. Further, $\{\beta_m \exp\left(-j2\pi f \tau_m\right)\}$ are not identically distributed, since the expected value $\mathbb{E}\left(|\alpha_{k,l}|^2\right)$ is proportional to $\exp\left(-T_l/\Gamma - \tau_{k,l}/\gamma\right)$. Since τ_m is a continuous random variable, $f\tau_m$ is also a continuous random variable. Then there exists an f that is large enough such that the distribution of $\exp\left(-j2\pi f \tau_m\right)$ can be approximated with a uniform distribution. Below, only such f is considered. Thus, the random variables $\{\beta_m \exp\left(-j2\pi f \tau_m\right)\}$ are uncorrelated.

The central limit theorem requires that the sum of the variances of the random variables goes to infinity when the number of random variables goes to infinity [15]. Thus, the central limit theorem does

not hold, since $\sum_{m=0}^{\infty} \mathbb{E}\left(|\beta_m|^2\right) < \infty$. However, if the variance of the random variables decays slowly enough, then a large number of random variables with significant variances contribute to the sum of the random variables. Then, it is reasonable to believe that the theorem still applies. If so, for a fixed f that is large enough, $C(f)$ converges in distribution to $C_I(f)+jC_Q(f)$, where $C_I(f)$ and $C_Q(f)$ are normally distributed with zero mean and variance σ^2, where σ^2 is to be determined. Thus, $|C(f)|^2$ is exponentially distributed with mean $2\sigma^2$.

The next step is to determine the variance σ^2. Let β_m^* be the complex conjugate of β_m. Then the expected value of $|C(f)|^2$ is obtained with

$$\begin{aligned}
\mathbb{E}\left(|C(f)|^2\right) &= \sum_{m=0}^{\infty}\sum_{n=0}^{\infty} \mathbb{E}\left(\beta_m\beta_n^* \exp\left(-j2\pi f(\tau_m-\tau_n)\right)\right) \\
&= \sum_{m=0}^{\infty}\sum_{n=0}^{\infty} \mathbb{E}\left(\beta_m\beta_n^*\right)\mathbb{E}\left(\exp\left(-j2\pi f(\tau_m-\tau_n)\right)\right) \\
&= \sum_{m=0}^{\infty} \mathbb{E}\left(\beta_m\beta_m^*\right)\mathbb{E}\left(\exp\left(0\right)\right) \\
&= \sum_{m=0}^{\infty} \mathbb{E}\left(|\beta_m|^2\right),
\end{aligned} \tag{17}$$

where the second last equality holds since $\mathbb{E}\left(\exp\left(-j2\pi f(\tau_m-\tau_n)\right)\right)$ $= \mathbb{E}\left(\exp\left(-j2\pi f\tau_m\right)\right)\mathbb{E}\left(\exp\left(j2\pi f\tau_n\right)\right) = 0$ when $m \neq n$. Thus,

$$\sigma^2 = \frac{1}{2}\sum_{m=0}^{\infty} \mathbb{E}\left(|\beta_m|^2\right). \tag{18}$$

The last step in estimating the distribution of G_{CIR} is started by defining the integral

$$J = \frac{1}{B}\int_{f_c-B/2}^{f_c+B/2} |C(f)|^2\, df, \tag{19}$$

which leads to $G_{\mathrm{CIR}} \approx X^2 J$. Assume that $|C(f)|^2$ is piecewise constant over a coherence bandwidth B_c. The number of subbands is $N_B = \lfloor B/B_c \rfloor$, where $\lfloor x \rfloor$ denotes the integer part of x. Within each subband, $|C(f)|^2$ is exponentially distributed with mean $2\sigma^2$. The integral J can then be approximated with

$$J \approx \tilde{J} = \sum_{p=0}^{N_B-1} \frac{J_p}{N_B}, \tag{20}$$

where $J_p = |C(f_c - B/2 + B_c(p+1/2))|$ for $p = 0, \ldots, N_B - 1$ are independent exponentially distributed with mean $2\sigma^2$ and variance

$4\sigma^4$. Further, $\{J_p/N_B\}$ have mean $2\sigma^2/N_B$ and variance $4\sigma^4/N_B^2$. Then $\tilde{J}$ has a gamma distribution $\Gamma(q,r)$ with $q = N_B$ degrees of freedom and parameter $r = 1/\mathbb{E}\left(J_p/N_B\right) = N_B/2\sigma^2$. The mean and variance of $\tilde{J}$ are $2\sigma^2$ and $4\sigma^4/N_B$, respectively.

Thus, the distribution of G_{CIR} can be approximated with a multiplication of two independent random variables, X^2 and $\tilde{J}$, which are log-normally and gamma distributed, respectively, i.e., $G_{\mathrm{CIR}} \approx X^2\tilde{J}$.

So far, the effect of the division with $\sqrt{G_\alpha}$ in (15) has not been considered in the calculation of $2\sigma^2$. This division gives that $\sum|\beta_m|^2$ is always one for all realizations. Consequently, the variance $\sigma^2 = 1/2$.

The random variables $\{J_p/N_B\}$ are independent identically distributed. If N_B is large enough, then the distribution of $\tilde{J}$ can be approximated with a random variable that has a normal distribution with mean $2\sigma^2$ and variance $4\sigma^4/N_B$. According to paper B, the average coherence bandwidth B_c of CM1–4 are around 32, 16, 11 and 6 MHz, respectively. With a bandwidth B equal to, e.g., 1500 MHz, the number of blocks N_B becomes 46, 93, 136, and 250 for CM1–4, respectively. As easily verified, the pdf of two random variables that are distributed with $\Gamma(N_B, N_B/(2\sigma^2))$ and $N(2\sigma^2, 4\sigma^4/N_B)$, respectively, are quite similar for $N_B = 50$. When N_B increases, the median of $\tilde{J}$ converges to the mean of $\tilde{J}$.

Different realizations have different ε_{pb}/N_0. The received power on the IEEE 802.15.3a chanel is $P_{r,\mathrm{UWB}} = P_{r,\mathrm{fs}}G_{\mathrm{CIR}}$, which gives $\varepsilon_{pb}/N_0 \approx P_{r,\mathrm{fs}}X^2\tilde{J}\mathrm{PG}/P_N$. Since $\sigma^2 = 1/2$, the mean received power is approximated with $\bar{P}_{r,\mathrm{UWB}} \approx P_{r,\mathrm{fs}}\mathbb{E}\left(X^2\right)$, which depends on the standard deviation of the shadowing σ_n. The expected value of G_{CIR} on the IEEE 802.15.3a channel model is given by

$$\bar{G}_{\mathrm{CIR}} = \mathbb{E}\left(G_{\mathrm{CIR}}\right) \approx \mathbb{E}\left(X^2\right)\mathbb{E}\left(\tilde{J}\right) = 10^{\sigma_n^2\ln(10)/200+\mu_n/10}2\sigma^2. \quad (21)$$

For $\mu_n = 0$, $\sigma_n = 3$, and $2\sigma^2 = 1$, $\bar{G}_{\mathrm{CIR}} \approx 1.27$ (1.04 dB).

Also, the distribution of $|C(f)|$ and $|H(f)|$ are Rayleigh and Suzuki, respectively, since X is log-normally distributed [16]. We have numerically verified, with high accuracy, that the estimated pdfs of the amplitude $|C(f)|$ and the phase $\angle C(f)$ are Rayleigh and uniformly distributed, respectively. Consequently, we expect that the performance of an uncoded OFDM system on CM1–CM4 and on a Rayleigh fading channel with uniformly distributed phase are the same.

If the bandwidth B increases, the performance of a system normally improves due to better diversity combination. However, as seen above, the increased bandwidth leads to less variation of G_{CIR}

and consequently to less variation of the received power. With fewer severe fading dips, the performance is expected to improve. The opposite happens when $B < B_c$, then we can expect that $\tilde{J}$ is exponentially distributed and that the receiver experiences a flat rayleigh fading channel.

4 Intrasystem Interference

One method of finding how much intrasystem interference a system can tolerate is to first decide a required PER of, e.g., 8%. Second, the required ε_{pb}/N_0 to achieve this PER without interference is found and is denoted γ_{req}. Then, in presence of interference, a new higher $\varepsilon_{pb}/N_0 = a\gamma_{\text{req}}$ where $a \geqslant 1$ is used. Finally, the minimum required signal-to-interference ratio (SIR) is found that gives the required PER of 8%. An increase of ε_{pb}/N_0 with a gives a decrease of the transmitter–receiver separation with $a^{1/n_{\text{plc}}}$, where n_{plc} is the path loss coefficient. Normal values of $10\log_{10} a$ are 1, 3, and 6 dB which corresponds to a decrease of the distances with a factor of 1.12, 1.41, and 2.0, respectively, for $n_{\text{plc}} = 2$.

The signal-to-interference ratio is given by $\text{SIR} = P_S/P_I$ where the P_S and P_I are the desired signal power and interference power, respectively. If two transmitters have the same transmit power, then $\text{SIR} = P_S/P_I = (d_I/d_S)^{n_{\text{plc}}}$, where d_S is the distance from the desired transmitter to the receiver and d_I is the distance from the interfering transmitter to the receiver.

Assuming that the contribution of the intrasystem interference after despreading is Gaussian and that it occupies the same RF bandwidth B as the desired signal, the power of the interference is $P_I = I_0 B$, where I_0 is the spectral density of the interference. Assume also that the noise bandwidth, the RF bandwidth, and that the chip rate are all equal, so that $B_N = B = R_c$. With $P_S = \varepsilon_{pb} R_b$, $\text{SIR} = (\varepsilon_{pb}/I_0)/\text{PG}$, where PG is the processing gain. The Gaussian interference assumptions gives that $\varepsilon_{pb}/(N_0 + I_0) = \gamma_{\text{req}}$. Since $(\varepsilon_{pb}/(N_0 + I_0))^{-1} = (\varepsilon_{pb}/N_0)^{-1} + (\varepsilon_{pb}/I_0)^{-1}$, it gives that $1/\gamma_{\text{req}} = 1/(a\gamma_{\text{req}}) + I_0/\varepsilon_{pb}$, which leads to $\varepsilon_{pb}/I_0 = \gamma_{\text{req}}(a/(a-1))$. Thus, the minimum required SIR is given by

$$\text{SIR} = \gamma_{\text{req}} \frac{a}{(a-1)\text{PG}}. \tag{22}$$

Clearly, if a better error correcting code is selected so that γ_{req} decreases with a coding gain G_c, then the required SIR drops with G_c. Normally, a higher data rate gives a lower processing gain, a lower coding gain and a higher required SIR.

The amount of intrasystem interference P_I that a system can handle depends only on the noise power P_N and a. Since $\varepsilon_{pb}/I_0 = (\varepsilon_{pb}/(N_0 + I_0))(a/(a-1))$ we get $I_0 = N_0(a-1)$ and

$$P_I = N_0 B(a-1) = P_N(a-1). \tag{23}$$

5 System Parameters

One packet contains $N_i = 8192$ information bits, i.e., 1024 bytes. A square root raised cosine (SRRC) pulse that was truncated at $\pm 6T_c$ with a roll-off factor of 0.2 was used. The arrival time in the receiver of the first path is assumed perfectly known. The implementation loss on the AWGN channel L_I and the noise figure N_F were assumed to be 3 dB and 7 dB, respectively. A decrease in L_I or N_F with θ dB increases the presented transmitter–receiver separation with a factor of $10^{\theta/(10n_{\text{plc}})}$, where $n_{\text{plc}} = 2$ is the path loss coefficient.

6 Numerical Results

An IEEE 802.15.3a channel realization $h(t)$ is time invariant during a connection but is completely different between connections. For each of the channel models CM1–CM4, the same 100 channel realizations were used. The presented PER on CM1–CM4 is the 90th-percentile PER, which is denoted PER_{90}. With a 90% probability, the obtained PER during a connection is lower than or equal to the presented PER_{90}. On the AWGN channel, there exits only one PER. See the beginning of Sec. 2.2.2 for more details.

When simulating on CM1–4, at least 200 packets for each channel realization were simulated. The simulation stopped when at least 50 packet errors had been obtained for the corresponding 90th-percentile PER.

The IEEE 802.15.3a channel model is a real-valued passband model. A continuous-time complex-valued baseband model was obtained with $h_{\text{BB}}(t) = h(t)\exp(-j2\pi f_c t)$, where f_c is the carrier frequency. In the simulations, a discrete-time baseband channel was used with a sampling frequency of two times the chip rate. When generating the channels, the arrival time of the first cluster T_0 was set to zero before generating the other arrival times $\{T_l\}$ and $\{\tau_{k,l}\}$ in (6). The sampler started sampling at the arrival time of the first path. This is not optimum for a chip-spaced receiver. The perfect channel estimate for a fractionally spaced rake combiner is defined here to be the same as the down-sampled complex baseband channel used in the simulations.

Numerical results for a single-band and a dual-band system are presented. First, results are presented for a single-band chip-spaced receiver that fulfills the IEEE 802.15.3a requirements on payload bit rates vs. distances. The dual-band system uses the same spectrum as the single-band system but divides it into two bands. The sampling rate of the single-band system and the dual-band system are equal. Thus, the dual-band system uses a fractionally spaced receiver with two times oversampling. In the dual-band system, a whole packet is transmitted in one of the two bands, i.e., no frequency hopping between the two band is used during the transmission of one packet. In terms of intrasystem interference, a dual-band system could become more resilient to intrasystem interference since one piconet might use the upper frequency band while another piconet uses the lower frequency band.

6.1 Required Chip Rate for the Single-Band System

After testing several chip rates, it was found that a single-band chip-spaced system with a rake combiner and a sliding window channel estimator is able to give a 90th-percentile PER of 8% with 1024 payload bytes for 110 Mbps at 10 meters on CM4. A chip rate R_c of 1540 Mchip/s and QPSK modulation were used. This sets the carrier frequency f_c to be 4.0 GHz which gives the -10 dB edges $f_{\min} \approx 3.14$ GHz and $f_{\max} \approx 4.86$ GHz.

For the single-band system, three information data rates R_b were investigated, 110 Mbps, 205 Mbps, and 513 Mbps, which correspond to the code rates 1/28, 1/15, and 1/6, respectively. For 110 Mbps, the outer convolutional code has rate 1/7 and the inner repetition code has rate 1/4. 205 Mbps is obtained with an outer code with rate 1/5 and an inner code with rate 1/3. Using only an outer convolutional code with rate 1/6 and no inner code, 513 Mbps is obtained. The constraint length of the convolutional codes are 7.

6.2 Link Budget for the Single-Band System

Tab. 2 shows the link budget for the single-band system on the AWGN channel. Definitions of the parameters can be found in Sec. 2.3 and the assumptions of N_F and L_I in Sec. 5. FCC set the maximum PSD $P_0 = 75$ nW/MHz [1]. Since B are assumed to be equal to R_c, the transmitted power P_t can be shown to be exactly $P_0 R_c$ for the untruncated SRRC pulse. The value of the roll-off factor does not affect P_t. This gives $P_t \approx -9.4$ dBm.

Tab. 2 shows the minimum required ε_{pb}/N_0 on the AWGN channel to give an 8% PER, Γ_{fs}. The values were obtained through

Table 2: Link budget for the single-band system on the AWGN channel.

Parameter	Value	Value	Value	Unit
Payload bit rate (R_b)	110	205	513	Mbps
Distance (d)	10	4	2	meter
Mean Tx Power (P_t)	−9.4	−9.4	−9.4	dBm
Tx antenna gain (G_t)	0	0	0	dBi
Free-space path loss ($L_p(d)$)	64.3	56.3	50.3	dB
Rx antenna gain (G_r)	0	0	0	dBi
Mean Rx power ($\bar{P}_{r,\mathrm{AWGN}}$)	−73.7	−65.7	−59.7	dBm
Thermal noise power (N_t)	−82.0	−82.0	−82.0	dBm
Rx noise figure (N_F)	7	7	7	dB
Implementation loss (L_I)	3	3	3	dB
Noise power (P_N)	−72.0	−72.0	−72.0	dBm
Processing gain (PG)	11.5	8.8	4.8	dB
SNR per payload bit (ε_{pb}/N_0)	9.8	15.0	17.1	dB
Req. ε_{pb}/N_0 AWGN (Γ_{fs})	3.3	3.5	3.4	dB
Rx sensitivity AWGN (Ψ)	−80.1	−77.2	−73.3	dBm
Link margin (M_L)	6.5	11.5	13.7	dB

simulations. The differences of up to 0.2 dB are due to the different coding gains of the convolutional codes. The Rx sensitivities on the AWGN channel Ψ for 110 Mbps at 10 meters, 205 Mbps at 4 meters, and 513 Mbps at 2 meters are −80.1, −77.2, and −73.3 dBm, respectively. This is the minimum required received power to give a PER of 8% on the AWGN channel. The link margins M_L are 6.5, 11.7, and 14.3 dB for the three rates, respectively. Each of them needs to be large enough so that a 90th-percentile PER of maximum 8% is obtained on the IEEE 802.15.3a channels for the same distance and payload bit rate. The system fulfills the IEEE 802.15.3a requirements on the AWGN channel since the link margins are positive.

6.3 Fingers and Pilots for the Single-Band System

For the requirement of 110 Mbps at 10 meters, only CM3 and CM4 are considered since they are valid at 10 meters, which CM1 and

Table 3: The number of pilots and rake fingers vs. the 90th-percentile PER for the single-band system.

Rate (Mbps)	d (m)	Channel	N_p pilots	N_R fingers	PER_{90}
110	10	CM4	16000	any	$> 8\%$
110	10	CM4	32000	60	7%
110	10	CM4	64000	55	7%
110	10	CM3	8000	17	7%
110	10	CM3	16000	16	7%
110	10	CM3	32000	16	6%

CM2 are not. It is more difficult to fulfill this requirement on CM4 than on CM3 since CM4 has the largest delay spread [6]. As seen in Tab. 3 and Fig. 2, $N_p = 16000$ pilots are not enough to obtain a PER less than 8%. A PER around 7% is obtained with 32000 pilots and 60 rake fingers or with 64000 pilots and 55 rake fingers. Since the negative slope of the curve of the PER vs. the number of rake fingers is rather small, the system has clear problems to fulfill the requirement on CM4. For CM3, Tab. 3 shows that 16 fingers with 16000 pilots or 17 fingers with 8000 pilots are enough to obtain an 8% PER. The negative slope of the curves of the PER vs. the number of fingers are much larger on CM3 than on CM4. This gives room for performance improvement by increasing the number of fingers on CM3. Note also the large difference in the required number of fingers and pilots between CM3 and CM4.

The required number of fingers and pilots for 205 Mbps at 4 meters are presented in Tab. 4 and Fig. 3. Here all four models CM1–4 are valid. With 32000 pilots on CM4, we see that only 12 fingers is enough, which is much less than the 60 fingers for 110 Mbps at 10 meters. Further, with 16000 pilots on CM3, the number of required fingers drops to 7. On CM1, i.e., a line-of-sight model between 1 and 4 meters, 1000 pilots and 3 fingers are enough. Adding more than 1000 pilots on CM1 does not decrease the number of required fingers. Even on CM2, 1000 pilots is enough with 5 fingers. Note the large difference in the required number of fingers and pilots between the different models at 4 meters with 205 Mbps.

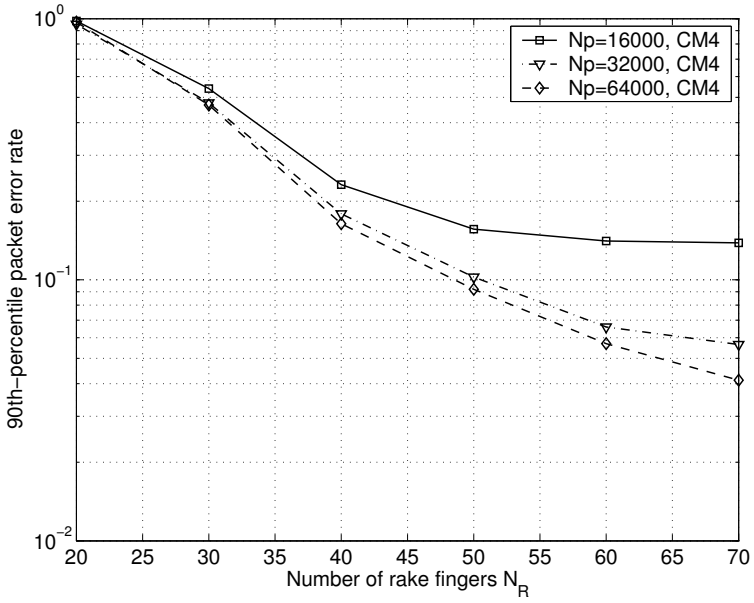

Figure 2: The 90th-percentile PER vs. the number of rake fingers for the single-band system on CM4 for 110 Mbps at 10 meters.

Table 4: The number of pilots and rake fingers vs. the 90th-percentile PER for the single-band system.

Rate (Mbps)	d (m)	Channel	N_p pilots	N_R fingers	PER_{90}
205	4	CM4	32000	12	6%
205	4	CM3	8000	7	7%
205	4	CM3	16000	7	5%
205	4	CM2	500	6	2.5%
205	4	CM2	1000	5	1.7%
205	4	CM2	2000	4	6%
205	4	CM2	4000	4	4%
205	4	CM2	8000	4	3%
205	4	CM1	500	4	4%
205	4	CM1	1000	3	8%
205	4	CM1	2000	3	7%
205	4	CM1	4000	3	5%
205	4	CM1	8000	3	3%

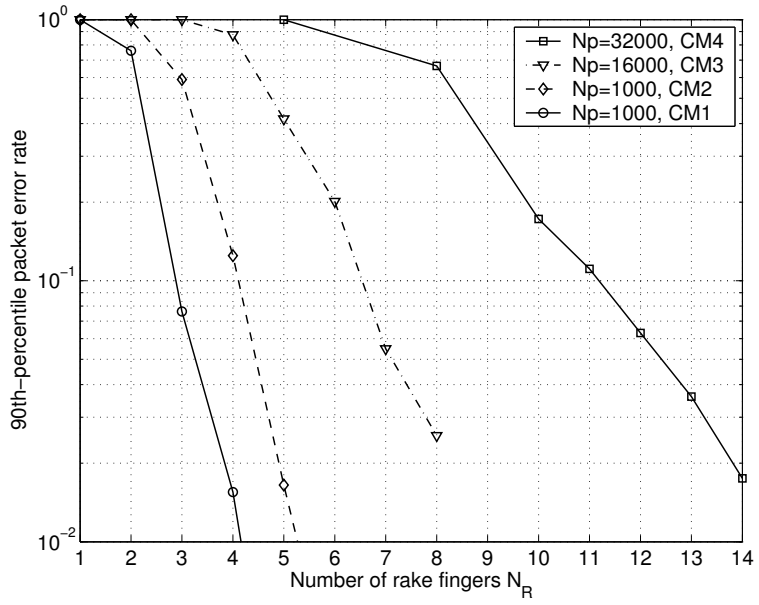

Figure 3: The 90th-percentile PER vs. the number of rake fingers for the single-band system for 205 Mbps at 4 meters.

6.4 Obtained Distances for the Single-Band System

Tab. 5 shows that the system gives a PER of 8% on the AWGN channel at 21 meters for 110 Mbps, 15.1 meters for 205 Mbps, and 9.7 meters for 513 Mbps. As expected, these distances are larger than the required 10, 4, and 2 meters since the link margins M_L in Tab 2 are positive.

Using 60 rake fingers and 32000 pilots, the system fulfills the requirements of at least 110 Mbps at 10 meters, at least 200 Mbps at 4 meters, and the optional one of at least 480 Mbps at 2 meters. A 90th-percentile PER less than 8% is obtained with 110 Mbps at 10 meters on CM4, 205 Mbps at 6.7 meters on CM4, and 513 Mbps at 3.8 meters at CM2. For details, please see Tab. 5 and Fig. 4. Since this setup fulfills all the requirements, it shows that the link margins M_L in Tab. 2 are sufficient.

If the requirement is relaxed so that only 110 Mbps at 10 meters is obtained on CM3 but not on CM4, the number of fingers can be reduced to 16 using only 16000 pilots, according to Tab. 5. Then only 7.4 meters is obtained on CM4 for 110 Mbps. However, this second setup gives 4.5 meters for 205 Mbps on CM4 and 2.9 meters for 513 Mbps on CM2, and thus this setup fulfills two out of three requirements.

Table 5: The obtained distances for the single-band system that gives an 8% PER using the 90th-percentile PER on CM1–CM4.

Rate (Mbps)	d (m)	Channel	Pilots N_p	Fingers N_R	Channel estimator
110	21.0	AWGN	0	1	Perfect
205	15.1	AWGN	0	1	Perfect
513	9.7	AWGN	0	1	Perfect
110	10.0	CM4	32000	60	SW
110	13.2	CM3	32000	60	SW
205	6.7	CM4	32000	60	SW
205	8.6	CM3	32000	60	SW
513	3.8	CM2	32000	60	SW
110	7.4	CM4	16000	16	SW
110	10.0	CM3	16000	16	SW
205	4.5	CM4	16000	16	SW
205	6.2	CM3	16000	16	SW
513	2.9	CM2	16000	16	SW

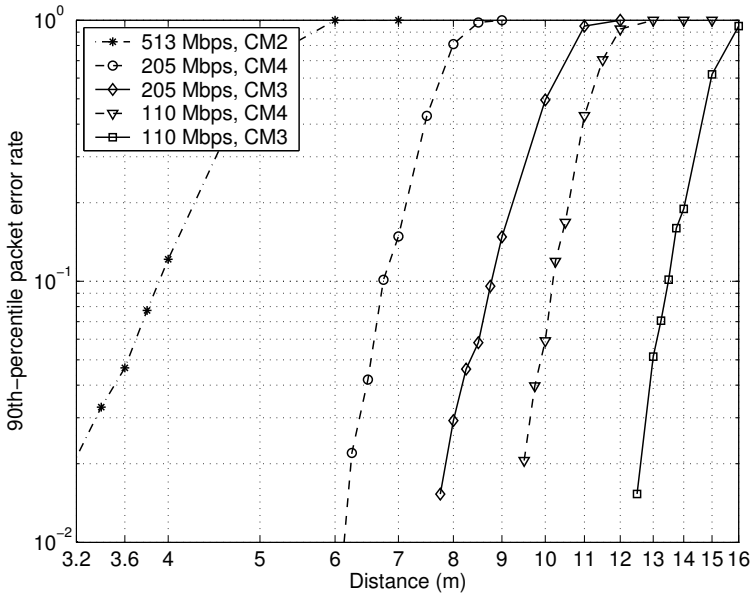

Figure 4: The 90th-percentile PER vs. distance for the single-band system with $N_R = 60$ fingers and $N_p = 32000$ pilots for 110, 205, and 513 Mbps.

Table 6: The required SIR for the single-band system when using $N_R = 60$ rake fingers and $N_p = 32000$ pilots.

Rate (Mbps)	d_S (m)	Channel	γ_{req} (dB)	SIR (dB)	d_I/d_S	d_I (m)
110	7.1	CM4	5.1	−3.3	0.68	4.8
110	9.4	CM3	4.7	−3.7	0.65	6.1
205	4.8	CM4	4.7	−1.0	0.89	4.2
205	6	CM3	6.6	0.9	1.1	6.6

6.5 Single-band Intrasystem Interference

Using 60 rake fingers and 32000 pilots, Tab. 6 shows the required SIR for 110 and 205 Mbps on CM3 and CM4. The values are obtained in the following way. For 110 Mbps at 10 meters on CM4, the channel impulse response gain G_{CIR} is 0.343 for the channel that gave the 90th-percentile PER. This gives the required $\gamma_{\text{req}} = \varepsilon_{pb}/N_0 = 5.1$ dB. When $a = 2$ (3 dB), the desired transmitter is $d_S = 10/\sqrt{2} = 7.1$ meters from the receiver that has an $\varepsilon_{pb}/N_0 = 8.1$ dB. According to (22), the minimum required SIR is −3.3 dB, which gives $d_I/d_S = 0.68$ and that the interfering transmitter is $d_I = 4.8$ meters from the receiver.

6.6 A Dual-Band System

As presented above, the single-band chip-spaced rake combiner with a chip rate of 1540 Mchip/s fulfills the IEEE 802.15.3a requirements on payload bit rates vs. T–R separations. Another approach is to divide the same spectrum 3.1–4.9 GHz that the single-band system uses into two bands. The lower band has $f_{\min} \approx 3.12$ GHz and $f_{\max} \approx 3.98$ GHz with $f_c = 3.55$ GHz. The upper band has $f_c = 4.45$ GHz, $f_{\min} \approx 4.02$ GHz, and $f_{\max} \approx 4.88$ GHz. The chip rate R_c for this dual-band system becomes 770 Mchip/s. By oversampling the analog signal with a factor of two, the sampling rate of the dual-band system is still 1540 Msamples/s as with the single-band system. The dual-band system uses a fractionally-spaced receiver.

The results for the dual-band system are presented in such a way that a connection between two transceivers uses either the lower or the upper band. Tab. 7 and Fig. 5 show the 90th-percentile PER vs. distance for the dual-band system at 110 Mbps. The fractionally-spaced rake combiner uses all available fingers on the channel and assumes perfect channel estimates. As seen, the system reaches

Table 7: The obtained distances for the dual-band system that gives a 90th-percentile PER of 8%.

Rate (Mbps)	d (m)	Channel	Band	Pilots N_p	Fingers N_R	Channel estimator
110	10.2	CM3	Lower	0	All	Perfect
110	8.1	CM3	Upper	0	All	Perfect
110	8.5	CM4	Lower	0	All	Perfect
110	6.9	CM4	Upper	0	All	Perfect
110	7.7	CM3	Lower	16000	16	SW
110	6.1	CM3	Upper	16000	16	SW
110	5.8	CM4	Lower	16000	16	SW
110	4.8	CM4	Upper	16000	16	SW

10.2 meters and 8.1 meters in the lower band and upper band, respectively, on CM3. This corresponds to a difference in SNR per bit of $10n_{\text{plc}}\log_{10}(10.2/8.1) = 2.0$ dB with $n_{\text{plc}} = 2$. On CM4, the system can have a transmitter–receiver separation of 8.5 and 6.9 meters in the lower and upper band, respectively. This corresponds to a 1.8 dB difference in SNR per bit between the bands.

Previously, a second setup for the chip-spaced single-band receiver was 16000 pilots and 16 rake fingers. When trying the same setup on the dual band system with the sliding window algorithm, Tab. 7 and Fig. 6 show that on CM3, 7.7 and 6.1 meters are obtained in the lower and upper band, respectively. For CM4, the distances are 5.8 and 4.8 meters, respectively. Note that $20\log_{10}(7.7/6.1) = 2.0$ dB and that $20\log_{10}(5.8/4.8) = 1.7$ dB. The geometric center frequency for the lower band $f'_{c,\text{lb}} \approx 3.52$ GHz and for the upper band $f'_{c,\text{ub}} \approx 4.43$ GHz. Since $20\log_{10}(f'_{c,\text{ub}}/f'_{c,\text{lb}}) \approx 1.99$ dB, it explains the observed differences of 2.0, 1.8, and 1.7 dB in SNR per bit.

The difference in SNR per bit on CM3 between the rake with all fingers and the rake with 16 fingers for the lower band and the upper band are $20\log_{10}(10.2/7.7) \approx 2.44$ dB and $20\log_{10}(8.1/6.1) \approx 2.46$ dB, respectively. On CM4, the losses are approximately 3.2 dB and 3.3 dB for the lower and upper band, respectively. It is reasonable that the loss is larger on CM4 due to its larger delay spread and since the same number of rake fingers are used on both CM3 and CM4.

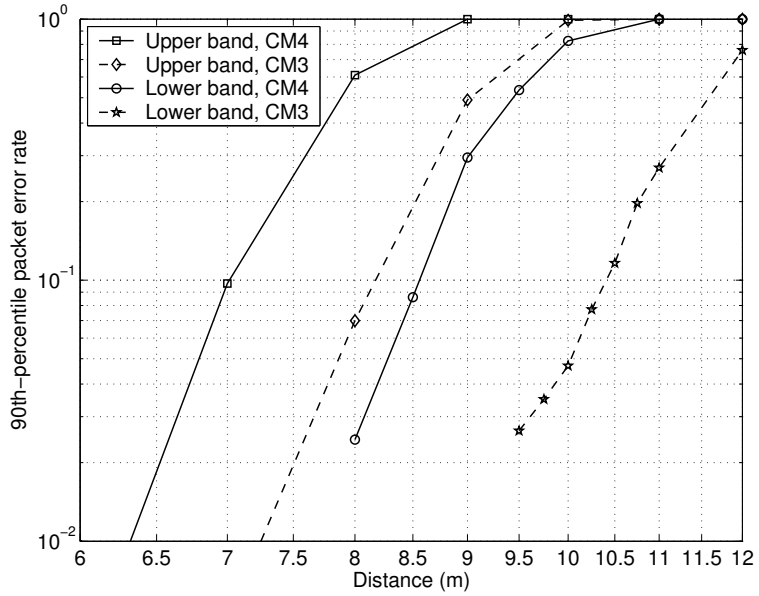

Figure 5: The 90th-percentile PER vs. distance for 110 Mbps using the dual-band system with a fractionally-spaced rake with all available fingers on the channel and perfect channel estimates.

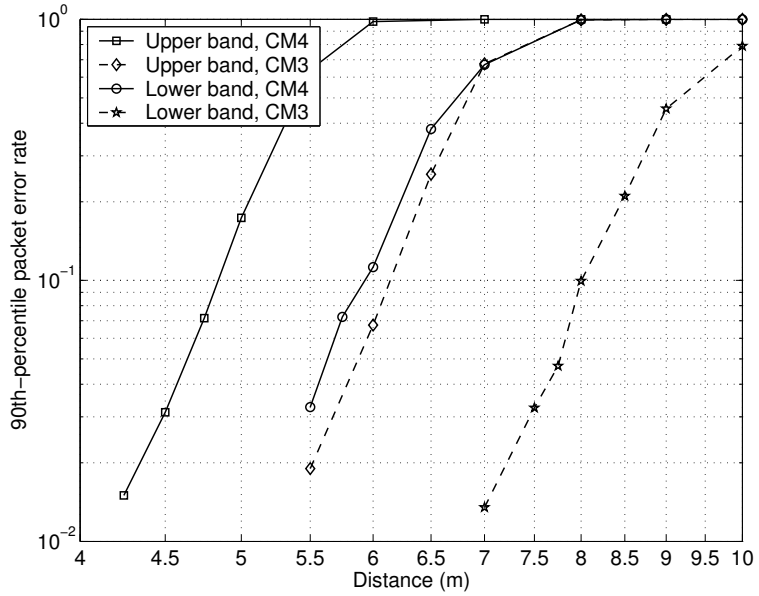

Figure 6: The 90th-percentile PER vs. distance for 110 Mbps using the dual-band system with a fractionally-spaced rake with 16 fingers, sliding window estimator, and $N_p = 16000$ pilots.

7 Discussion

7.1 Transceiver Algorithms

A sliding window (SW) channel estimator is maximum-likelihood (ML) optimal for a one-tap channel or if the autocorrelation of the pilot sequence is a Dirac pulse, i.e., the pilot sequence is white. Unfortunately, neither of these two requirements is valid in the investigated systems, which results in a performance loss for to the selected channel estimation algorithm compared with an ML-estimator.

The scrambling in the digital transmitter block makes the payload signal pseudo-white, which is necessary for the rake combiner to function. However, since the autocorrelation of the scrambling sequence is not a Dirac pulse, the signals from the rake fingers are correlated before the addition. Thus, the theoretical performance of MRC is not obtained. After the combination of the signals, interchip interference will be introduced. Further, the chip-matched filter and the rake combiner together form the matched filter to the received waveform of one transmitted chip. With a perfect channel estimate and an infinite number of taps, the rake combiner maximizes the SNR for each chip, which is not the same as maximizing the signal to noise and chip interference.

A fractionally spaced receiver can compensate for channel distortion due to intrapulse interference by sampling at least as fast as the Nyquist rate. A chip-spaced receiver introduces aliasing. A fractionally spaced receiver is also much less sensitive to synchronization errors than chip-spaced receivers since each pulse is oversampled. Chip-spaced receivers have problems with finding the optimum sampling point.

7.2 Packet Error Rates

Here, we will illustrate four packet error rate measures when the log-normal shadowing X in (6) is included or not, respectively. Some intuitive explanations can be drawn after observing the influence of shadowing and the length of the preamble on the different PER measures and what slope to expect. In Sec. 6, three packet error rate measures are defined, the 90th-percentile PER, the mean PER, and the mean PER of the 90% best channels. They are denoted, PER_{90}, $\overline{\mathrm{PER}}$, and $\overline{\mathrm{PER}}_{90}$, respectively. A fourth measure is the median PER that is given by $\mathbb{P}\left(\mathrm{PER} < \mathrm{PER}_{50}\right) = 0.5$. Fig. 7 and 8 show the four measures vs. the SNR per payload bit on the AWGN channel ε_{pb}/N_0 with $G_{\mathrm{CIR}} = 1$ in (12).

As expected, based on the definitions of the PER measures,

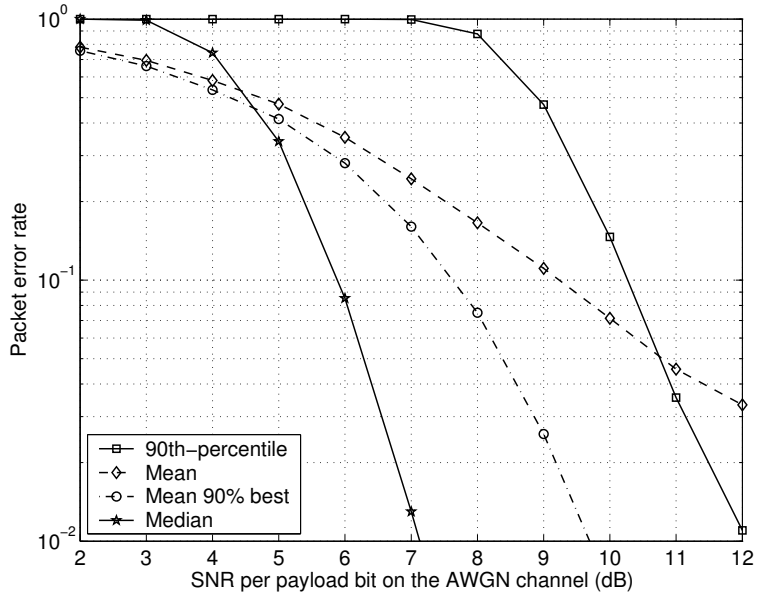

Figure 7: Illustration of the four different packet error rate definitions on CM3 with the log-normal shadowing X.

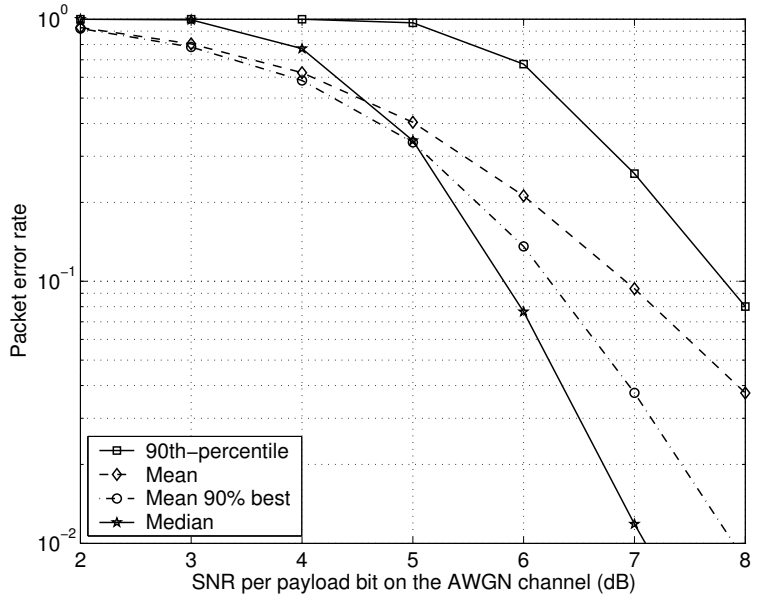

Figure 8: Illustration of the four different packet error rate definitions on CM3 without the log-normal shadowing X.

Fig. 7 and 8 illustrate that, for any given distance, the 90th-percentile PER is always larger than the mean PER of the 90% best channels and the median PER. Also, the mean PER is always larger than the mean PER of the 90% best channels. For any distance d, the median packet error rate is unaffected by the log-normal shadowing and its standard deviation σ_n. However, the mean PER and the 90th-percentile PER depend on σ_n.

As seen in Fig. 8, without log-normal shadowing, the 90th-percentile PER is not equal to the median PER on the IEEE 802.15.3a channel, since different CIRs without the shadowing give different PERs. Assume that we have channel where only the shadowing affects the PER and the CIR does not. The 90th-percentile PER is then $\Phi^{-1}(0.9)\sigma_n \approx 3.84$ dB worse than the median PER. Here, $\Phi(t) = \int_{-\infty}^{t} \exp\left(-x^2/2\right)\, dx/\sqrt{2\pi}$.

If a system gives certain median, mean, and 90th-percentile packet error rates at a distance d, then those packet error rates are unaffected if a preamble of any length is added. The SNR per payload bit ε_{pb}/N_0 controls the different PERs and is unaffected by the preamble length. If we add pilots beyond the number where the performance does not improve, the distance and the packet error rate will not be affected. However, the effective throughput decreases.

We can expect that the slope for high SNR of the median PER and the 90th-percentile PER to be equal in presence of shadowing as seen in Fig. 7. Since the mean PER is obtained by averaging over the pdf of the PER, the negative slope of the mean PER is less than the negative slope of the 90th-percentile PER. There are probably a few bad channels that highly affect the mean PER.

8 Conclusions

The first objective of this paper is to find the system specifications for a single-band system that fulfills the physical layer requirements from IEEE 802.15.3a. The system should provide at least 110 Mbps at 10 meters and at least 205 Mbps at 4 meters. An optional requirement is at least 480 Mbps at 2 meters. The second objective is to investigate the performance of a dual-band system that uses the same spectrum and sampling rate as the single-band system.

The investigated single-band system with a chip rate of 1540 Mchip/s can provide a payload bit rate of 110 Mbps at 10 meters on CM4, 205 Mbps at 6.7 meters on CM4, and 513 Mbps at 3.8 meters on CM2, which fulfills the requirements from IEEE 802.15.3a. At those distances, the 90th-percentile PER is 8% with 1024 payload

bytes. A chip-spaced rake combiner with a sliding window (SW) channel estimator, 60 rake fingers, and 32000 pilots was used. The receiver sensitivities on the free space path loss channel are -80.1, -77.2, and -73.3 dBm for 110 Mbps at 10 meters, 205 Mbps at 4 meters, and 513 Mbps at 2 meters, respectively. For 110 Mbps, the receiver requires an SIR of -3.3 dB when the transmitter is 7.1 meters from the receiver on CM4.

A dual-band system with a chip rate of 770 Mchip/s, a fractionally spaced rake combiner using all available rake fingers on the channel, and perfect channel estimates gives 10.2 meters on CM3 in the lower band. When using 16 rake fingers and the SW algorithm, the 110 Mbps at 10 meters requirement is not fulfilled on CM3 and CM4. It is important to note that for every 1 dB increase of the noise figure or the implementation loss, the obtained distance decreases with a factor of 1.122.

A channel impulse response gain is defined. Based on assumptions that the central limit theorem holds, it is proven that the gain can be approximated with multiplication of a log-normally distributed random variable and a gamma distributed random variable.

Acknowledgment

This work has been funded by Ultrawaves, PCC++, and the Swedish Research Council. The authors would like to express their gratitude to the partners in Ultrawaves for sharing their expertise in UWB systems.

References

[1] "Revision of part 15 of the commission's rules regarding ultra-wideband transmission systems," Federal Communications Commission, First Report and Order, ET Docket 98–153, Apr. 2002.

[2] A. Batra et al., "TI physical layer proposal for IEEE 802.15 task group 3a," Doc. no. P802.15-03/142r1-TG3a, IEEE P802.15 WPAN, May 2003, available at `http://grouper.ieee.org/groups/802/15/`.

[3] A. Batra et al., "Multi-band OFDM physical layer proposal for IEEE 802.15.3a," Sept. 2004, available at `http://www.multibandofdm.org`.

[4] R. Roberts, "XtremeSpectrum CFP document," Doc. no. P802.15-03/154r3, IEEE P802.15 WPAN, July 2003, available at `http://grouper.ieee.org/groups/802/15/`.

[5] R. Fisher et al., "DS-UWB physical layer submission to 802.15 Task Group 3a," Doc. no. P802.15-04/137r3, IEEE P802.15 WPAN, July 2004, available at `http://grouper.ieee.org/groups/802/15/`.

[6] J. Foerster et al., "Channel modeling sub-committee report final," Doc. no. P802.15-02/490r1-SG3a, IEEE P802.15 WPAN, Feb. 2003, available at `http://grouper.ieee.org/groups/802/15/`.

[7] A. Saleh and R. Valenzuela, "A statistical model for indoor multipath propagation," *IEEE Journal on Select. Areas Commun.*, vol. 5, pp. 128–137, Feb. 1987.

[8] M.-O. Wessman, ed., "D4.1: Transceiver study and preliminary design report," Doc. no. W04-03-0017-P04, Ultrawaves, Apr. 2003, available at `http://www.ultrawaves.org`.

[9] B. Mielczarek, M.-O. Wessman, and A. Svensson, "Performance of coherent UWB rake receivers with channel estimators," *IEEE VTC'03 fall*, Oct. 2003.

[10] M.-O. Wessman et al., "D4.2: Transceiver design and link level simulation results," Doc. no. W04-03-0025-R07, Ultrawaves, Dec. 2003, available at `http://www.ultrawaves.org`.

[11] M.-O. Wessman et al., "D4.2: Transceiver design and link level simulation results - part II, rev II," Doc. no. W04-03-0025-R14, Ultrawaves, Dec. 2004, available at `http://www.ultrawaves.org`.

[12] J. Ellis et al., "P802.15.TG3a alt PHY selection criteria," Doc. no. P802.15-03/031r11, IEEE P802.15 WPAN, May 2003, available at `http://grouper.ieee.org/groups/802/15/`.

[13] J. Ellis et al., "TG3a technical requirements," Doc. No. P802.15-03/030r0, IEEE P802.15 WPAN, Dec. 2002, available at `http://grouper.ieee.org/groups/802/15/`.

[14] J. G. Proakis, "Adaptive equalization for TDMA digital mobile radio," *IEEE Trans. Veh. Tech.*, vol. 40, no. 2, pp. 333–341, May 1991.

[15] G. R. Grimmett and D. R. Stirzaker, *Probability and random processes,* Oxford University Press, 3rd ed., 2001.

[16] H. Suzuki, "A Statistical Model for Urban Radio Propagation," *IEEE Trans on Comm.*, vol. 25, no. 7, pp. 673–680, July 1977.

[17] M.-O. Wessman, A. Svensson and E. Agrell, "Frequency Diversity Performance of Coded Multiband-OFDM Systems on IEEE UWB Channels," *IEEE VTC'04 fall*, Sept. 2004.